

JGR Earth Surface

RESEARCH ARTICLE

10.1029/2024JF008204

Key Points:

- Long-term natural erosion rates were higher in the Upper Ayeyarwady than in the Upper Chindwin (0.06–0.34 mm/a vs. 0.02 mm/a)
- Present-day erosion rates are higher in the Upper Chindwin (0.63 ± 0.05 mm/a), where they increased by more than one order of magnitude
- Anthropogenic activities represent an important contributor to sediment discharge of the modern Ayeyarwady River

Supporting Information:

Supporting Information may be found in the online version of this article.

Correspondence to:

X. Hu and G. Li,
huxm@nju.edu.cn;
guangweili@nju.edu.cn

Citation:

Dong, X., Hu, X., Li, G., Garzanti, E., Najman, Y., Liang, W., et al. (2025). Accelerated erosion and sediment fluxes in the Ayeyarwady River due to anthropogenic activities. *Journal of Geophysical Research: Earth Surface*, 130, e2024JF008204. <https://doi.org/10.1029/2024JF008204>

Received 3 DEC 2024

Accepted 10 JUL 2025

Author Contributions:

Funding acquisition: Xiumian Hu, Guangwei Li

Methodology: Jiangan Wang

Software: Xiaolong Dong, Yuntao Tian

Supervision: Xiumian Hu, Guangwei Li

Visualization: Xiaolong Dong,

Xiumian Hu, Guangwei Li

Writing – original draft: Xiaolong Dong

Writing – review & editing:

Xiaolong Dong, Xiumian Hu,

Guangwei Li, Eduardo Garzanti,

Yani Najman, Wendong Liang,

Yuntao Tian, Jiangan Wang

Accelerated Erosion and Sediment Fluxes in the Ayeyarwady River Due To Anthropogenic Activities

Xiaolong Dong¹, Xiumian Hu¹ , Guangwei Li¹ , Eduardo Garzanti² , Yani Najman³ , Wendong Liang⁴ , Yuntao Tian⁵ , and Jiangan Wang⁶ 

¹State Key Laboratory of Critical Earth Material Cycling and Mineral Deposits, School of Earth Sciences and Engineering, Nanjing University, Nanjing, China, ²Laboratory for Provenance Studies, Department of Earth and Environmental Sciences, University of Milano-Bicocca, Milano, Italy, ³Lancaster Environment Centre, Lancaster University, Lancaster, UK, ⁴State Key Laboratory of Oil and Gas Reservoir Geology and Exploitation, Institute of Sedimentary Geology, Chengdu University of Technology, Chengdu, China, ⁵Guangdong Provincial Key Lab of Geodynamics and Geohazards, School of Earth Sciences and Engineering, Sun Yat-sen University, Guangzhou, China, ⁶State Key Laboratory of Lithospheric and Environmental Coevolution, Chinese Academy of Sciences, Institute of Geology and Geophysics, Beijing, China

Abstract Human activities have a strong impact on global climate and natural ecosystems, yet the extent of their influence on long-term natural erosional processes remains poorly determined. A quantitative analysis is needed. The Ayeyarwady River, renowned for its large sediment flux ranking second in Asia, provides a compelling case study. We here show that extensive anthropogenic activities in the Ayeyarwady catchment have strongly accelerated erosion rates compared to natural benchmark levels, thereby contributing to its high sediment discharge. To highlight this point, we compared present-day erosion rates calculated from sediment fluxes with long-term natural erosion rates derived from detrital-apatite fission track (AFT) and cosmogenic ¹⁰Be data. Our findings reveal a stark contrast. Long-term natural erosion rates were notably higher in the Upper Ayeyarwady (0.06–0.34 mm/a) than in the Upper Chindwin (0.02 ± 0.005 mm/a), whereas present-day erosion rates are three times higher in the Upper Chindwin (0.63 ± 0.05 mm/a) than in the Upper Ayeyarwady (0.19 ± 0.02 mm/a). Particularly, noteworthy are the Upper Chindwin and Mu drainages, where erosion rates are calculated to have increased by more than an-order-of-magnitude relative to long-term natural background rates. Such a striking increase in erosion rate correlates positively with the spatial distribution of alluvial mining, especially for the Upper Chindwin catchment. The observed increases in sediment fluxes from long-term to present-day timescales may also be attributed to land-use expansion related deforestation, and intensified precipitation. These results underscore how human activities can drastically accelerate erosional processes, thus exerting a dramatic impact on natural systems.

Plain Language Summary Human activities are known to significantly affect global climate and natural ecosystems, but their impact on long-term erosional processes remains to be quantitatively assessed. In this study, we show that extensive alluvial mining in the Ayeyarwady catchment has strongly accelerated erosion compared to natural background levels, thereby contributing to its very high sediment discharge. By comparing modern erosion rates with long-term natural erosion rates, we discovered a major discrepancy. Natural erosion rates were much higher in the Upper Ayeyarwady basin than in the Upper Chindwin basin. But, in stark contrast, present-day erosion rates are three times higher in the Upper Chindwin than in the Upper Ayeyarwady. The erosion rates in the Upper Chindwin and Mu drainage basins are calculated to have increased by more than one order of magnitude relative to past natural erosion rates. These findings reveal a strong link between mining and increased sediment discharge, with land-use expansion related deforestation, and increasing precipitation in the 20th-century making contributions to all Ayeyarwady sub-catchments. This study shows that human activities can dramatically accelerate erosion, strongly impacting sediment discharge, natural landscapes, and ecosystems.

1. Introduction

Human activities can significantly influence erosion at decadal to annual timescales thus accelerating sediment production in river catchments by deforestation (e.g., in the southern Ecuadorian Andes; Vanacker et al., 2007), agricultural land use (e.g., Sri Lanka; Hewawasam et al., 2003), and alluvial mining (e.g., global tropical rivers; Dethier et al., 2023). Recent remote-sensing research has shown that alluvial mining has notably increased

extensive jade and gold mining (Shrestha et al., 2020) was not considered. To investigate the potential anthropogenic impact, a combined approach is applied to quantify the human-induced increment of sediment production relative to natural background values by comparing present-day to long-term natural erosion rates. Present-day erosion rates were calculated directly from gauged suspended-load and reported modeled bedload data wherever available (Cohen et al., 2022), combined with forward mixing modeling (Garzanti et al., 2012) in sub-catchments where gauged data are unavailable. Long-term natural erosion rates were inferred from both numerical inversion of detrital apatite fission track (AFT) ages (million-year timescale) and cosmogenic ^{10}Be (thousand-year timescale). The comparison of these independent data sets highlights how the very high present-day sediment fluxes in the Ayeyarwady River largely result from anthropic activities. This study thus underscores the impact that human activities may have on the acceleration of erosion and sediment fluxes in large river systems.

2. The Ayeyarwady River

The Ayeyarwady River (drainage basin $\sim 430,000\text{ km}^2$) flows southward across Myanmar for $\sim 2,170\text{ km}$ and forms a large delta distributary network before discharging into the Andaman Sea. The Upper Ayeyarwady originates from the confluence of the Nmai and Mali headwater branches, both sourced from high mountain glaciers in northernmost Myanmar, $\sim 280\text{ km}$ southeast of the eastern Himalaya syntaxis (Figures 1a and 1b). The Upper Ayeyarwady upstream of the Chindwin confluence is joined from north to south by the Taping, Shweli and Myitnge left-bank tributaries, and farther downstream by the Mu River near Sagaing. The principal tributary by far is the Chindwin River, which runs southward along the eastern edge of the Indo-Myanmar Ranges (IMR), receives its left-bank Uyu and right-bank Myitha tributaries, and finally joins the Ayeyarwady River to the southeast of Mandalay. Only minor tributaries contribute to the Lower Ayeyarwady between the Chindwin confluence and the sea.

2.1. Hydrology and Sediment Flux

Most of the Ayeyarwady basin is dominated by the southwest Asian monsoon and thus characterized by a tropical monsoonal climate, with most precipitation and discharge between June and September (Zaw et al., 2017). Rainfall varies markedly across the basin, from $\sim 500\text{ mm}$ in central areas to $4,000\text{ mm}$ in northern mountainous regions (Sirisena et al., 2021) (Figure 1c). The average and maximum water discharge are estimated to be $12,000$ and $42,100\text{ m}^3/\text{s}$, respectively (Baronas et al., 2020).

The Ayeyarwady River is less regulated compared to other major rivers in Asia, such as the Yangtze, Mekong, or Salween (Dethier et al., 2022; Wang et al., 2011). There are no large dams on the main river and only small dams exist in a few tributaries (Schmitt et al., 2021). The annual suspended-load flux of the Ayeyarwady River at Pyay was estimated to be $326 + 91 - 70$ million tons (Mt) in 2017–2019 (Baronas et al., 2020), consistent with previous estimates of $325 \pm 57\text{ Mt}$ (Furuichi et al., 2009) and $364 \pm 60\text{ Mt}$ (Robinson et al., 2007). Notably lower figures (265 Mt) were estimated in the nineteenth-century (Gordon, 1885). The two main branches, the Chindwin and the Upper Ayeyarwady, contributed annually $\sim 120\text{ Mt}$ at Kalewa over the period 1991–2010 (Sirisena et al., 2021) and $\sim 64\text{ Mt}$ at Sagaing (International Finance Corporation, 2017), between 1990 and 2010.

2.2. Geological Background

The Ayeyarwady catchment can be subdivided into four main geological domains (Figure 1b): the IMR in the west, the Central Myanmar Basin (CMB), the Mogok Metamorphic Belt (MMB) in the north, and the Shan Plateau in the east. The IMR, located to the west of the Kabaw Fault, is a Mesozoic-Cenozoic accretionary prism (Betka et al., 2018), comprising Triassic schists, Jurassic ophiolites, and Cretaceous sedimentary rocks in the IMR core (Brunnschweiler, 1966; Suzuki et al., 2004), Eocene sedimentary rocks in the Inner IMR (Mitchell, 1993; Naing et al., 2014), and Neogene strata in the Outer IMR (Allen et al., 2008). The CMB hosts a $\geq 10\text{-km}$ -thick Cretaceous to Quaternary forearc and backarc basin succession accumulated in various depocenters separated by the mid-Cretaceous-Miocene Wuntho-Popa Arc (Kyaw Linn et al., 2015; Licht et al., 2020). The MMB is an elongated domain of up to high-grade metamorphic rocks and Permian to Miocene granitic intrusions, separated by the ophiolite-bearing belt from the Precambrian metamorphic basement and Triassic turbidites of the Katha Gangaw Range in the west (e.g., Mitchell et al., 2012) (Figure 1b). The easternmost domain, the Shan Plateau,

exposes Neoproterozoic-Paleozoic sedimentary rocks intruded by Cambrian to Mesozoic granitoids (Bender, 1983).

3. Sampling and Methods

In 2013 and 2020, 15 fine to medium sand samples were collected from active fluvial bars along the Ayeyarwady River and its major tributaries from northern Myanmar headwaters to the Ayeyarwady Delta. Sampling sites were selected away from the tributaries confluence and urban or village areas to make samples representative. Prior to collection, the top 10 cm of surface sand was removed to minimize wind disturbance effects. Ten new sand samples were analyzed for framework petrography and heavy minerals, while five headwater samples, previously analyzed by Garzanti et al. (2016), were also included. Additionally, 13 samples were selected for detrital AFT analysis, and nine were used for cosmogenic ^{10}Be measurement. Full information on sample locations is provided in Tables S1 in Supporting Information S2.

3.1. Petrography and Heavy Minerals Analysis

Ten sand samples (seven from the mainstem and one each from the Chindwin, Mu, and Yaw rivers) were analyzed for petrography and heavy minerals to calculate a provenance budget (Tables S2, S3 in Supporting Information S2). From each sand sample, a quartered fraction of the 63–2,000 μm class obtained by wet sieving was impregnated with araldite epoxy and cut into a standard thin section. Petrographic analyses were carried out by counting more than 400 points on each thin section according to the Gazzi-Dickinson method (Ingersoll et al., 1984). Sand classification was based on the relative abundance of the three main framework components quartz (Q), feldspars (F), and lithic fragments (L), considered if exceeding 10% QFL (Garzanti, 2019).

From a split aliquot of the 32–500 μm size window obtained by wet sieving, heavy minerals were separated by centrifuging in Na-polytungstate (2.90 g/cm^3). More than 200 transparent heavy minerals (tHM) were point-counted at appropriate regular spacing to minimize overestimation of smaller grains (Garzanti & Andò, 2019). Dubious grains were checked by Raman spectroscopy (Andò & Garzanti, 2014). The source rock density (SRD; g/cm^3) index is the weighted average density of terrigenous grains calculated from point-counting mineralogical data. According to the transparent-heavy-mineral concentration (tHMC) in the sample, tHM suites are defined as very poor (tHMC < 0.5), poor ($0.5 \leq \text{tHMC} < 1$), moderately poor ($1 \leq \text{tHMC} < 2$), moderately rich ($2 \leq \text{tHMC} < 5$), rich ($5 \leq \text{tHMC} < 10$) or very rich (tHMC ≥ 10) (Garzanti & Andò, 2007). The complete data set is provided in Tables S2 and S3 in Supporting Information S2.

3.2. Apatite Fission Track (AFT) Analysis and Calculation of Erosion Rates at Million-Year Timescale

Detrital AFT analyses were performed on 13 sand samples using the LA-ICP-MS method (Hasebe et al., 2004). Polished mounts embedded with apatite grains were etched in 5 M HNO_3 at 20°C for 20 s to reveal spontaneous fission tracks (Barbarand et al., 2003). Fission track counting was carried out using a Zeiss Axio Imager M2m microscope. Stacks of high-resolution digital images of each selected grain were then captured by TrackWorks with a $\times 100$ dry objective under both transmitted and reflected light using a highly sensitive and fast iDS camera at Nanjing University. Track counting was performed manually in *FastTracks* using the coincidence mapping technique (Gleadow et al., 2009). The etch pit diameter (D_{par}) of the selected grains was also determined. Uranium concentration in each counted grain was determined by LA-ICP-MS using an Agilent 8900 ICP-QQQ with an ESI New Wave NWR 193UC (TwoVol2) laser ablation system at the Beijing Quick-Thermo Science and Technology Co., Ltd. NIST SRM 612 glass was used to calibrate trace elements using calcium as internal standard. Reference materials were analyzed twice before and after each analytical session, each time including 8 spots. Ablation on selected grains and reference materials was carried out for 30 s after ~ 10 s baseline signal collection, using a 30 or 40 μm diameter beam size according to apatite grain size, operated at $\sim 3 \text{ J}/\text{cm}^2$ fluence with 5 Hz repetition rate. Because of large uncertainties, apatite grains with uranium concentration < 2 ppm were excluded from further analysis. In this study, 1,270 single-grain AFT ages were obtained from 13 samples (Figure 3); 35 grains were excluded from age calculations because of their low uranium concentration (< 2 ppm) and consequently high age uncertainties. The complete data sets are provided in Tables S4 in Supporting Information S2.

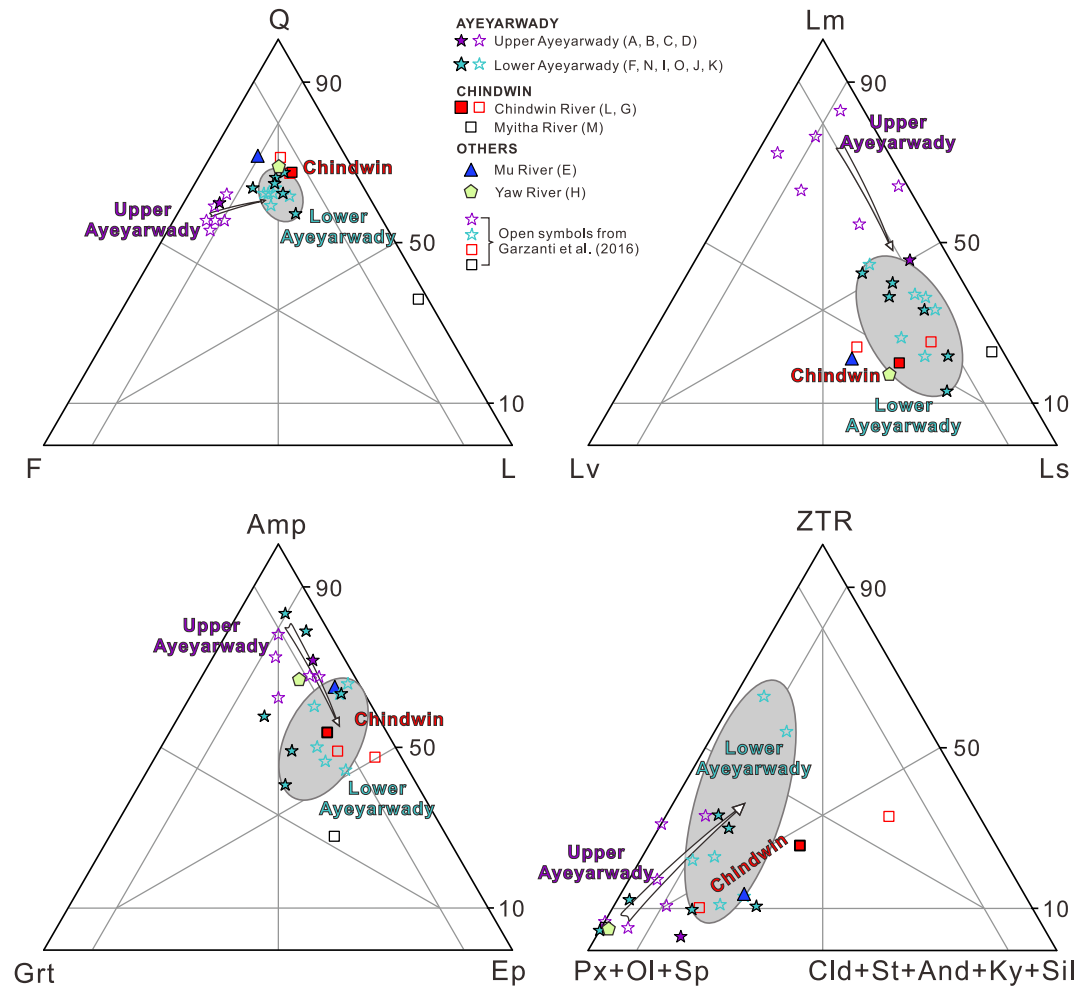


Figure 2. Petrographic composition and heavy-mineral suites of the Ayeyarwady River sands. *Q* = quartz; *F* = feldspars; *L* = lithic fragments (*Lv* = volcanic; *Lm* = metamorphic; *Ls* = sedimentary, compositional fields after Garzanti et al., 2016); *Amp* = amphibole; *Grt* = garnet; *Ep* = epidote-group; *ZTR* = zircon + tourmaline + rutile; *Px* = pyroxene; *Ol* = olivine; *Sp* = Cr-spinel; *Cl* = chloritoid; *St* = staurolite; *And* = andalusite; *Ky* = kyanite; *Sil* = sillimanite. Gray shaded ovals indicate the cluster of Lower Ayeyarwady. Capital letters refer to sample sites (see Figure 1b).

3.3. Calculation of Catchment-Wide Erosion Rates at Million-Year Timescales From Detrital Cooling Ages

Million-year timescale exhumation rates were obtained from inversion modeling of detrital AFT ages based on the age-elevation relationship. Fission-induced damage tracks in apatite are annealed at temperatures over 60–120°C (Gallagher et al., 1998), so that fission-track ages reflect cooling associated with exhumation from crustal depths of 2–5 km. We employed a Bayesian estimation of erosion model implemented with MATLAB (Avdeev et al., 2011), which has been shown to efficiently invert temporally variable erosion histories from detrital dates. The applied approach relies on the primary assumption that sands were derived from a catchment with a monotonic positive thermochronological age-elevation (or depth) relationship. Based on this assumption and using a detritus sampling function, a distribution of detrital dates can be predicted. To compare predictions against observations, the goodness of the assumed age-elevation (or depth) relationship was evaluated and optimized through computational iterations. Finally, a catchment erosional history was derived from the slopes of the optimal age-elevation (or depth) relationship, as illustrated in previous studies (Ye et al., 2022; Zhuang et al., 2018).

We assumed a vertical exhumation pathway and a flat closure isotherm, so that bedrock ages are a function of elevation only (Duvall et al., 2012). This allows us to infer the age-elevation relation of source catchment from

detrital ages [that is, for the observed detrital ages t_i ($i = 1, 2, 3, \dots, p$), we retrieved the elevations z_i ($i = 1, 2, 3, \dots, p$) in the source area]. The elevation points were sampled by the Markov chain Monte Carlo (MCMC) algorithm (e.g., Avdeev et al., 2011; Duvall et al., 2012). According to each t - z path, the detrital ages can be converted into elevation points, allowing the derivation of its probability distribution function.

For N detrital ages, we assume that these particles are uniformly distributed across the watershed. Therefore, the elevation distribution of these particles should represent a sample chosen from the overall watershed elevation data (i.e., the elevation distribution of the particles and the watershed elevations are assumed to be independent and identically distributed). Consequently, we selected N elevation samples from the watershed and assigned age values to these samples based on their elevation in increasing order, thus obtaining the age-elevation curve. To determine whether the cumulative probability function (CDF) of these chosen points matches that of the source catchment hypsometry, we turned to the two-sample Kuiper test that is (relatively to the Kolmogorov-Smirnov test) insensitive to the tails of the distribution and guarantees equal sensitivities to all variable values (Kuiper, 1962; Vermeesch, 2007a, 2007b). We used the Kuiper test at the 95% significance level (Ruhl & Hodges, 2005; Vermeesch, 2007a, 2007b) and chose the most proper t - z path that the best collapsed the CDF of the source catchment. Accordingly, the slope of the t - z path is the erosion rate of the source area. We choose the last stage slope of the t - z path as the million-year erosion rate. Because the monotonic positive thermochronological age-elevation relationship assumption is not valid for the Chindwin basin, the western margin of which consists of a thrust belt (the Kabaw Fault in Figure 1b, Burma Earth Sciences Research Division, 1977a), we applied this approach only to the upper Ayeyarwady catchment.

3.4. ^{10}Be -Derived Basin-Averaged Erosion Rates at Thousand-Year Timescales

Quartz grains were separated from the 125–500 μm size window of nine sand samples following standard magnetic, heavy-liquid, and acid dissolution procedures at the University of Melbourne (Schaefer et al., 2022). The ^{10}Be concentrations were then measured by accelerator mass spectrometry at the Australian National University. Erosion rates were calculated according to Zhang et al. (2017). In a steadily eroding landscape with rock density ρ_r (calculated according to point-counting data), the catchment-averaged erosion rate (ϵ) is:

$$\epsilon = (P_{\text{avg}}\Lambda)/(N\rho_r) \quad (1)$$

where N is the ^{10}Be concentration in sediment, P_{avg} is the average production rate within the catchment, and Λ is the production attenuation scale in rock ($\sim 160 \text{ g cm}^{-2}$) (Lal, 1991). Solving Equation 1 for ϵ requires estimates of P_{avg} . Using the Microsoft Excel calculator *Cosmocalc* (Vermeesch, 2007a, 2007b), we scaled the cosmogenic nuclide production rates for each pixel ($\sim 30 \times \sim 30 \text{ m}$) from SRTM-DEM data for both elevation and latitude to obtain the catchment-averaged production rate (Lal, 1991; Stone, 2000). The shielding factor related to catchment topography was calculated using the algorithm of Codilean (2006). Results are reported in Tables S6 in Supporting Information S2.

3.5. Calculation of Present-Day Erosion Rates

Present-day erosion rates can be directly calculated from sediment fluxes, catchment areas, and average density of source rocks (SRD index obtained from quantitative mineralogical data in the absence of hydraulic-sorting effects; Garzanti & Andò, 2007). For sub-catchments where gauging data were not available, we partitioned gauged sediment fluxes in the mainstem by forward mixing modeling based on integrated petrographic and heavy-mineral data (Garzanti et al., 2012). The forward mixing model assumes that the compositional signature of detritus derived from each end-member source is known accurately; then, the relative amount of sediment contributed by diverse tributaries or distinct geological domains (endmembers) can be quantitatively assessed by independent forward-mixing calculations. For each river basin, the composition of detritus (petrography and heavy minerals) derived exclusively from each single geological unit was considered as an endmember.

After the relative contributions from different parent sources (e.g., catchments) to a daughter sediment were calculated using the mixing model, they were partitioned among the different sources according to the sediment flux (Mt/a), and a sediment budget was obtained. The average density (g/cm^3) of the exposed source rocks was calculated according to sand mineralogy (SRD index of Garzanti & Andò, 2007). Erosion rates for each source (mm/a) can be finally calculated as the ratio between the sediment yield and the average density of exposed rocks

(g/cm^3). Detailed method, rationale, and endmember choices for forward mixing modeling are described in full in Text S2 in Supporting Information S1. The sediment yield is the sum of bedload and suspended load normalized by dividing by the upstream drainage area. Bedload fluxes were adopted from literature modeling data calculated using the *WBMsed* model (Cohen et al., 2022).

4. Results

4.1. Petrography and Heavy Minerals

Upper Ayeyarwady sand is feldspatho-quartzose with plagioclase > K-feldspar, minor phyllite, schist, and felsitic volcanic rock fragments, and abundant mica (mostly biotite). The rich transparent-heavy-mineral (tHM) suite is dominated by hornblende and epidote, with minor garnet, pyroxene, kyanite, and Cr-spinel (Figure 2). The Chindwin River, by contrast, carries feldspatho-litho-quartzose sand with more quartz and lithic fragments (shale, sandstone, chert, felsitic and microlitic volcanic, phyllite/schist, and serpentine-schist types), and less mica. The moderately rich tHM suite consists of amphibole, clinopyroxene and epidote with subordinate garnet, kyanite, minor zircon, rutile, enstatite, and rare apatite.

The Mu River draining the CMB and the Wuntho-Popa Arc carries litho-feldspatho-quartzose sand with abundant felsitic volcanic and sedimentary rock fragments, and rare metamorphic rock fragments. The moderately poor tHM suite includes mainly amphibole and epidote, with subordinate garnet, kyanite, pyroxene, and minor zircon, rutile, and apatite. The Yaw River draining the IBR and CMB carries feldspatho-litho-quartzose sand with plagioclase \approx K-feldspar. Felsitic volcanic and metavolcanic, shale, sandstone, and chert rock fragments are common; mica is rare. The moderately rich, amphibole-dominated tHM suite includes clinopyroxene, epidote, garnet, minor zircon, titanite, and apatite.

Lower Ayeyarwady feldspatho-litho-quartzose sand is compositionally similar to Chindwin sand (Figure 2) and contains more plagioclase than K-feldspar, mainly pelite, sandstone, slate, phyllite, schist, felsic volcanic, and minor serpentinite-schist lithics, and common mica (mostly biotite). The moderately rich tHM suite mainly consists of amphibole and epidote with garnet, pyroxene, and minor kyanite, Cr-spinel, zircon, titanite, and apatite.

4.2. Detrital AFT Results

The Upper Ayeyarwady is characterized by notably younger detrital AFT ages than the Chindwin River (Figure 3), consistent with thermochronological ages of bedrock sources (Figure 1e). In the Upper Ayeyarwady (samples A, B, C, D), single-grain AFT ages range from 538 Ma to 1.8 Ma, with the main peak at \sim 9 Ma (Figure 3; Tables S5 in Supporting Information S2). More than 90% of the grains are younger than 30 Ma, half being younger than 10 Ma.

In the Upper Chindwin River, detrital AFT ages (samples L and G) range from 549 to 3.2 Ma, with major peaks around 10 Ma and 19 Ma, and minor peaks at 33, 59, and 77 Ma. About one-third of the ages are younger than 15 Ma and another third are older than 30 Ma. A similar distribution of AFT ages, ranging from 84.4 to 4.4 Ma with the main peak at \sim 19 Ma and minor peaks at \sim 28, \sim 40, and \sim 58 Ma, characterizes the Yaw River in the south (sample H; Figure 3). Apatite in the Myitha River (sample M) yielded even older ages, with the main peak at \sim 19 Ma. A similar distribution of AFT ages, ranging from 97.5 to 7.1 Ma, with the main peak at \sim 16 Ma and a minor peak at \sim 30 Ma, characterizes the Mu River (sample E).

The Ayeyarwady River shows more AFT ages older than 20 Ma (\sim 35%) downstream of the Mu confluence (sample F). Downstream of the Chindwin confluence (samples I, J, K, Figure 3), the detrital AFT age distribution becomes similar to that characterizing the Chindwin River, with ages ranging from 127 to 1.4 Ma, the main peak around 13–17 Ma and minor older peaks.

4.3. Million-Year Timescale Erosion Rates

Erosion rates at the million-year timescale of Upper Ayeyarwady catchments were obtained through numerical inversion of detrital AFT ages. Since the Chindwin River, draining the IMR, has the bimodal detrital AFT signature, which reflects the activations of different sub-units of IMR (the 19 Ma population from the Paleogene IBR and the 10 Ma population from the IMR core according to Najman et al., 2020, 2022). We only applied the

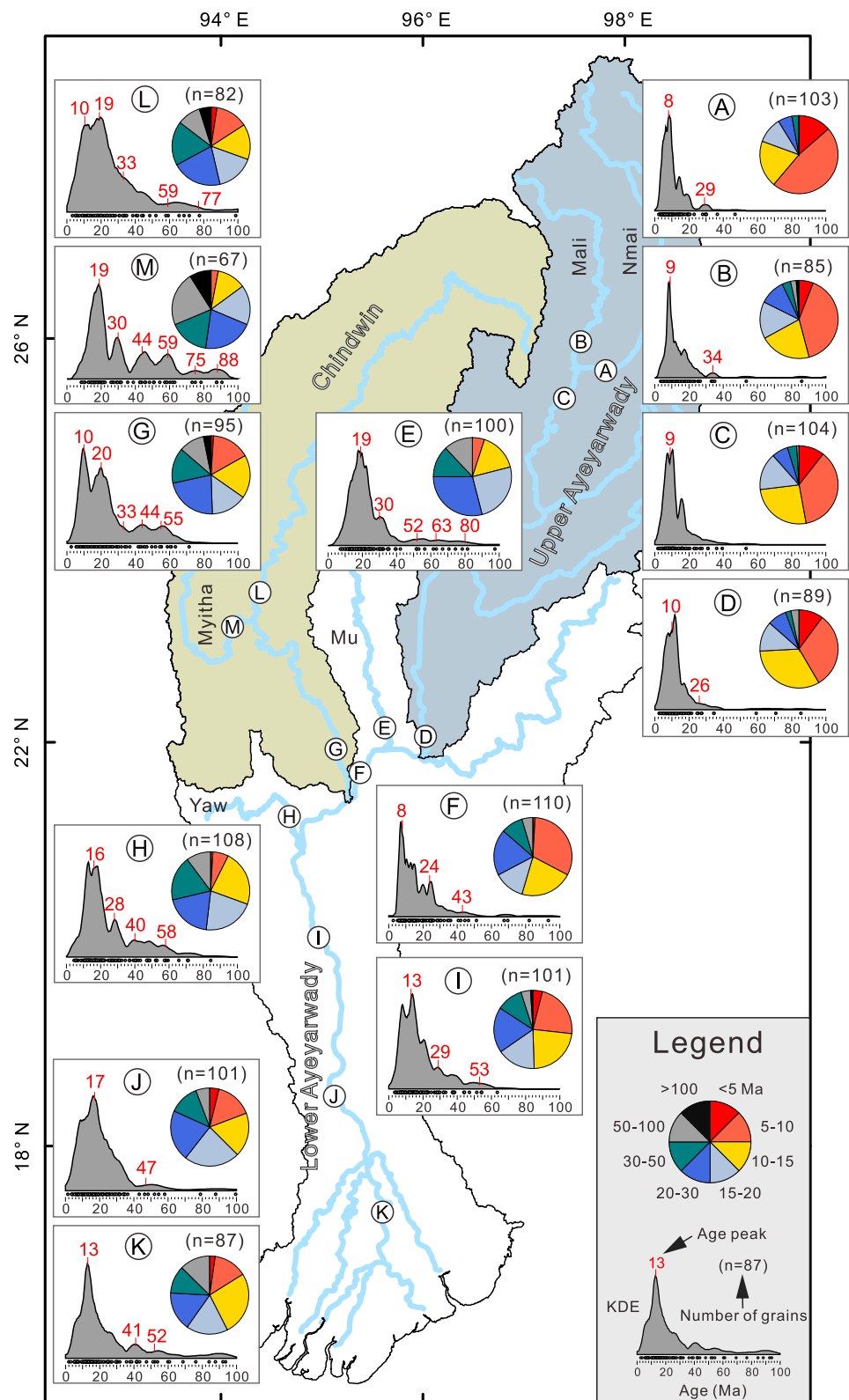


Figure 3. Kernel Density Estimates of measured apatite fission track age distributions plotted with *DensityPlotter* (Vermeesch, 2012). Pie charts represent relative abundances of different age groups (see legend).

inversion modeling method on two small Ayeyarwady tributaries (samples A, B), and two Upper Ayeyarwady samples C and D (see Figure 1b).

The Nmai subcatchment exhibits the highest rate ($0.34 + 0.04 - 0.03$ mm/a; Figure 4a), followed by the Mali subcatchment (0.10 ± 0.01 mm/a; Figure 4b). Lower rates are inferred for the Upper Ayeyarwady mainstream ($0.06 - 0.07$ mm/a; Figures 4c and 4d).

4.4. ^{10}Be Results

The ^{10}Be concentration in quartz grains across the Ayeyarwady catchment ranges from $(2.9 \pm 1.0) \times 10^4$ atoms/g to $(15.2 \pm 3.0) \times 10^4$ atoms/g with the highest values recorded in the Upper Chindwin (Tables S6 in Supporting Information S2). As for AFT data, ^{10}Be -derived erosion rates (Figure 5) indicate higher denudation in the Upper Ayeyarwady (from 0.06 mm/a to 0.26 ± 0.06 mm/a) than in the Chindwin catchment (from 0.02 ± 0.005 mm/a to 0.12 ± 0.04 mm/a), with highest rates in the Nmai (0.26 ± 0.06 mm/a) and Mali catchments (0.12 ± 0.03 mm/a) and lowest rates in the Upper Chindwin (0.02 ± 0.005 mm/a) and Mu catchments (0.05 ± 0.01 mm/a) (Figures 5 and 6b). The ^{10}Be -derived basin-wide erosion rate calculated here for the entire Ayeyarwady (0.10 ± 0.03 mm/a) is slightly lower than a previous ^{10}Be -derived estimate (0.19 ± 0.03 mm/a) (Wittmann et al., 2020), and much lower than the neighboring Brahmaputra (1.0–1.1 mm/a) (Lupker et al., 2017) and Ganga rivers (0.7–1.2 mm/a) (Lupker et al., 2012) draining the Himalayan Range (Figures 5 and 6b).

5. Discussion

5.1. Long-Term Natural Erosion Rates

Natural erosion rates at the million-year and thousand-year timescales are broadly consistent in the Upper Ayeyarwady catchment (0.06–0.34 mm/a vs. 0.06–0.24 mm/a). Within this catchment, the Mali and Nmai drainages have the highest erosion rates at both million-year (0.10–0.34 mm/a) and thousand-year timescales (0.12–0.26 mm/a). The Upper Ayeyarwady exhibits higher rates than the Upper Chindwin catchment in the thousand-year timescale, as indicated by ^{10}Be data (0.06–0.26 mm/a vs. 0.02 ± 0.005 mm/a) (Figures 5 and 6a, 6b). The erosion rate in the Upper Chindwin catchment is the lowest (0.02 mm/a) of all locations studied at the thousand-year timescale, while the Lower Chindwin shows higher erosion rates (0.12 mm/a).

These spatial variations in the long-term erosion rates show no significant—and even a slightly negative—correlation with lithological erodibility ($p = 0.08$, Figure 7c), indicating that high sediment fluxes cannot be entirely related to source-rock erodibility as previously hypothesized (Garzanti et al., 2016). However, the erosion rates can be adequately explained by climate, topography and tectonics. Long-term natural erosion rates exhibit a positive correlation with catchment-averaged precipitation ($R^2 = 0.46$, $p = 0.01$, Figure 7b). They also show a weak positive correlation with drainage area weighted average k_{sn} values of bedrock rivers ($R^2 = 0.34$, $p = 0.1$, Figure 7a; river morphometry analysis is provided in Text S1 in Supporting Information S1 and results are listed in Table S8 in Supporting Information S2), intimately associated with topography and regional tectonics. Our calculated timing and extent of erosion are compatible with the tectonic history of the region. The MMB, located in the northeastern part of the Irrawaddy catchment (represented by the Nmai and Mali rivers), has experienced exhumation in the Late Oligo-Miocene as determined from mica Ar-Ar dating (Bertrand et al., 2001). This is consistent with the timing of exhumation shown for the region of the Mali River catchment as determined through inversion modeling of our detrital AFT data (Figure 4b, increase from 0.03 to 0.10 mm/a at 24 Ma). Little low temperature thermochronological data are published for this region. However, Lei et al. (2006) showed AFT data from adjacent Yunnan that may be consistent with the younger rapid exhumation we calculate through inversion modeling of our detrital AFT data from the Nmai catchment (increase from 0.14- to 0.34 mm/a) at 9.9 Ma (Figures 4a and 6a). By contrast, the Chindwin catchment lies outwith the region of the MMB, and the lower ^{10}Be -derived thousand-year erosion rates of the upper Chindwin reflect this. The higher values of the lower Chindwin likely reflect input from the Myitha River draining the western IMR (erosion rates in thousand-year timescale 0.11 mm/a; Figure 6b), although it has previously been calculated that this river only contributes 5% of sediment to the modern Chindwin River (Garzanti et al., 2016).

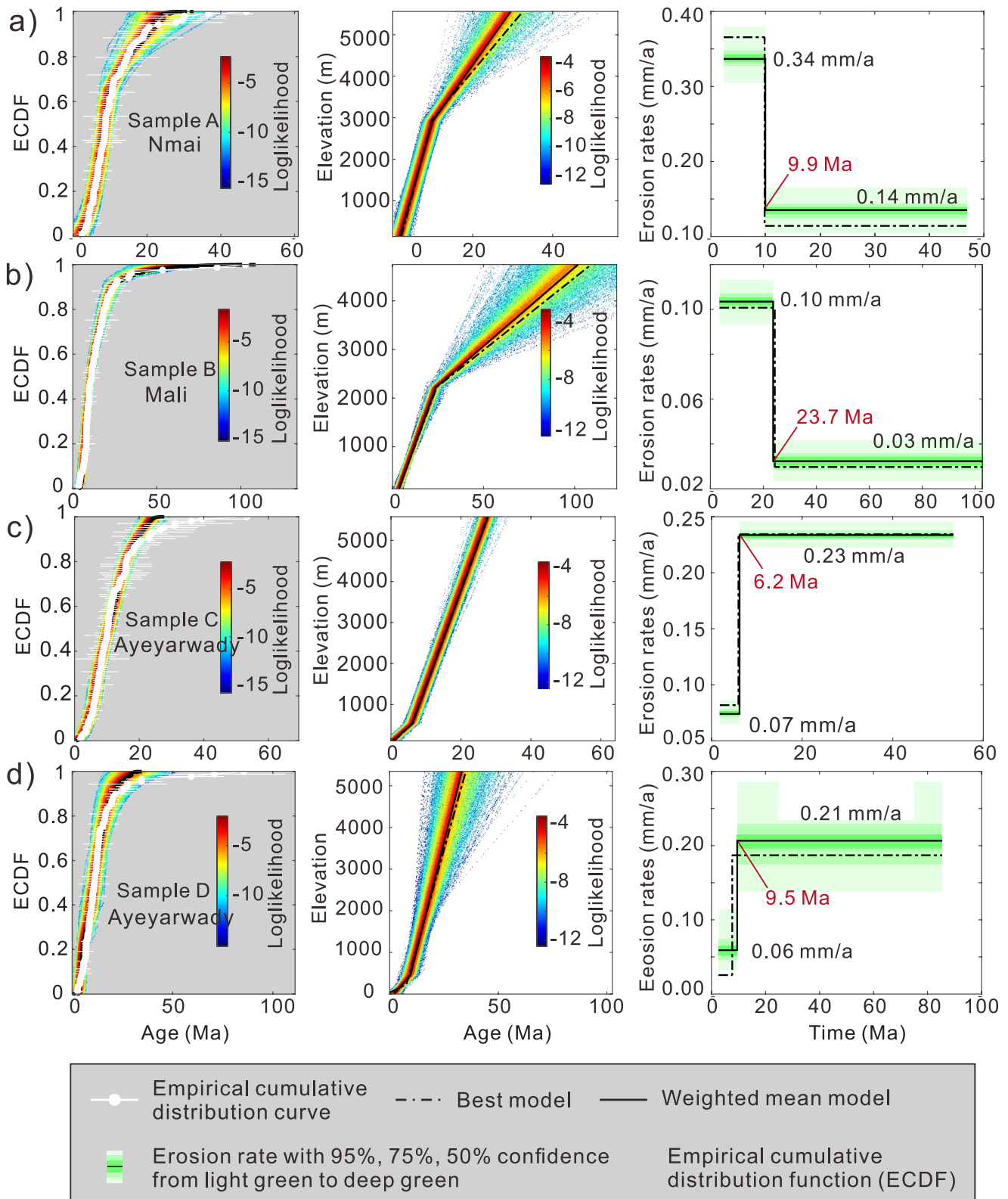


Figure 4. Numerical modeling results of Upper Ayeyarwady (a–d). Bedrock exhumation history is derived from detrital apatite fission track data under different erosion models.

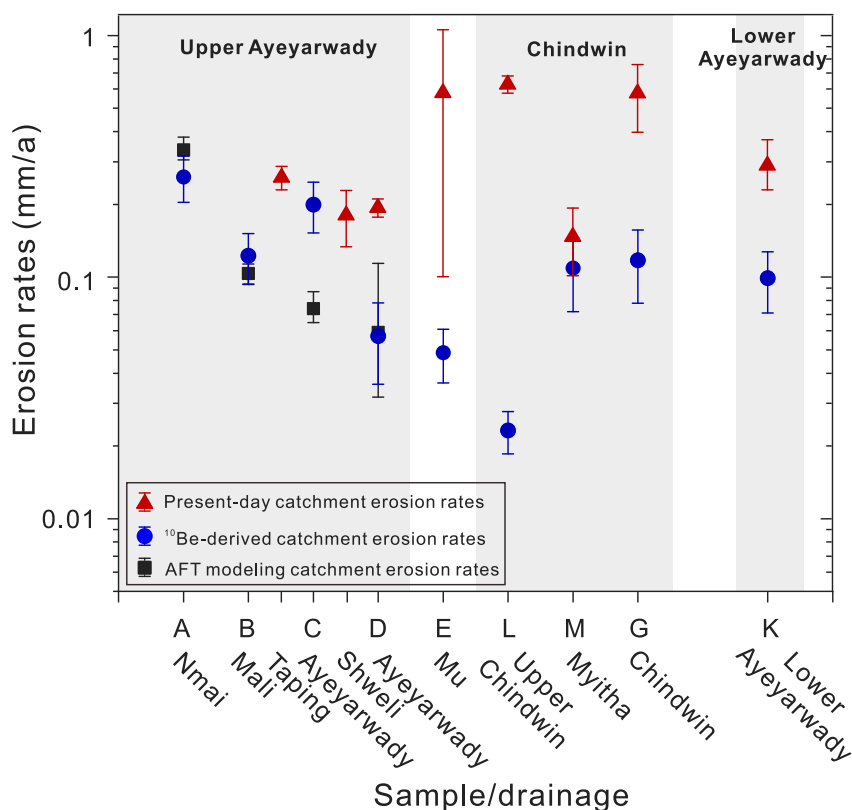


Figure 5. Comparison of erosion rates at different timescales.

5.2. Present-Day Erosion Rates

The composition of Ayeyarwady sand changes significantly downstream of the Chindwin confluence (Figure 2), indicating prominent sediment supply from the Chindwin River. Forward-mixing calculations based on integrated bulk-petrography and heavy-mineral data indicate that sediment in the Lower Ayeyarwady is contributed $38 \pm 6\%$ by the Upper Ayeyarwady, $9 \pm 7\%$ to the Mu River, and $53 \pm 7\%$ to the Chindwin River. These results are consistent with previously calculated contributions of $45 \pm 17\%$ from the Upper Ayeyarwady and of $55 \pm 17\%$ from the Chindwin River (Garzanti et al., 2016). The Myitha River is estimated to supply only $\sim 5\%$ of the Chindwin River sediments, and the Yaw River makes negligible contributions to the Lower Ayeyarwady.

The suspended sediment flux calculated using forward mixing modeling is similar to the gauged sediment flux in the Upper Chindwin (120 ± 9 Mt/a vs. 164 ± 51 Mt/a) but higher than the gauged data in the Upper Ayeyarwady (123 ± 40 Mt/a vs. 64 ± 5 Mt/a). Additionally, suspended sediment fluxes calculated by forward mixing modeling are consistent with *WBMed* modeling results (Cohen et al., 2022), indicating that our calculations are reliable (Tables S7 in Supporting Information S2).

Present-day erosion rates thus calculated are 0.19 ± 0.02 mm/a for the Upper Ayeyarwady, 0.58 ± 0.48 mm/a for the Mu River, 0.63 ± 0.05 mm/a for the Chindwin River upstream of the Myitha confluence, 0.58 ± 0.18 mm/a for the entire Chindwin catchment, and $0.29 + 0.08\text{--}0.06$ mm/a for the entire Ayeyarwady catchment. Similar rates are estimated for the Shweli (0.18 ± 0.05 mm/a) and Taping (0.26 ± 0.03 mm/a) tributaries to the Upper Ayeyarwady (Figures 5 and 6c).

5.3. Present-Day versus Long-Term Natural Erosion Rates

In the Upper Ayeyarwady catchment, the long-term natural erosion rates at million-year and thousand-year timescales are broadly consistent (Figure 7e), but for the entire Ayeyarwady catchment, present-day erosion rates have increased drastically and by different degrees in different sub-catchments (Figure 7f). The strongest increase is displayed by the Upper Chindwin catchment, where present-day erosion rates are calculated to have

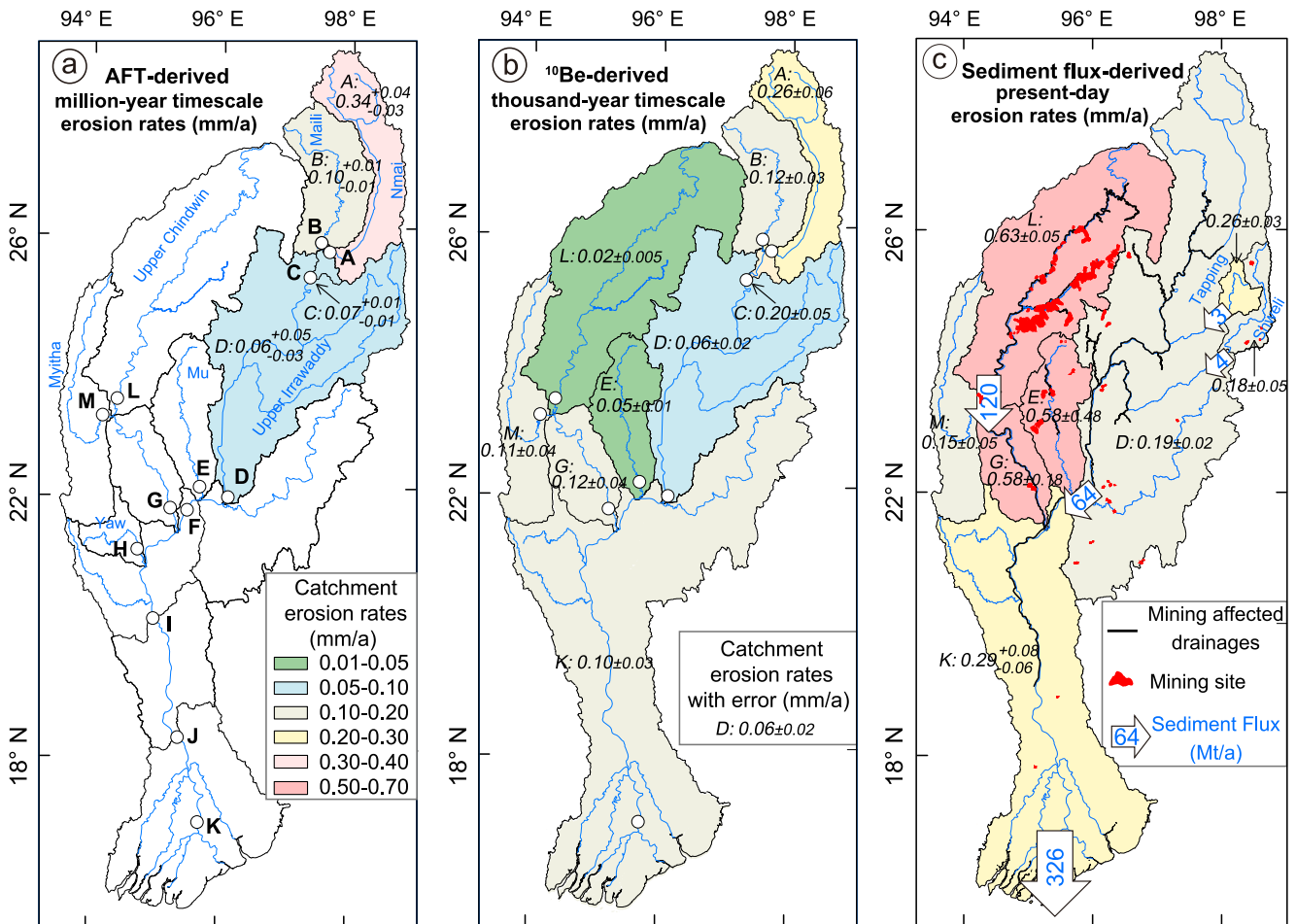


Figure 6. Erosion rate maps of the Ayeyarwady drainage at different timescales. (a) million-year timescale rate based on detrital apatite fission track numerical modeling; (b) thousand-year timescale rate based on ^{10}Be concentration in quartz grains; (c) present-day rate based on gauged sediment fluxes combined with forward mixing modeling. Remote sensing data on alluvial mining (Maus et al., 2022) and mining-affected drainages (Dethier et al., 2023) are highlighted in red. Sources of gauged sediment data: Upper Chindwin at Kalewa (1991–2010) (Sirisena et al., 2021); Upper Ayeyarwady at Sagaing (1990–2010, IFC, 2017); Upper Shweli and Upper Taping from Chinese Hydrological Yearbooks (1958–1987).

risen by a factor of 32 (from 0.02 ± 0.005 mm/a to 0.63 ± 0.05 mm/a) relative to the long-term erosion rate. An increase by a factor of five is recorded for the entire Chindwin catchment (from 0.12 to 0.58 mm/a), and by a factor of three for the Upper Ayeyarwady (from 0.06 to 0.19 mm/a). The present-day rate also trebled for the entire Ayeyarwady (0.29 ± 0.08 – 0.06 mm/a) compared to the ^{10}Be -derived long-term rate (0.10 ± 0.03 mm/a) (Figures 5 and 6b, 6c). Most noteworthy, present-day erosion rates are three times higher in the Upper Chindwin (0.63 ± 0.05 mm/a) compared to the Upper Ayeyarwady (0.19 ± 0.02 mm/a), marking a clear reversal compared to long-term erosion patterns (Figures 5 and 6b and 6c).

Thus, in contrast with the long-term erosion patterns, the Chindwin River has presently replaced the Upper Ayeyarwady as the major sediment contributor to the Lower Ayeyarwady. Whilst we acknowledge that different approaches have been used to calculate the erosion rates over the different timescales, we do not consider that differences of approach can explain the variation we record. Different approaches have been used over various time scales to calculate erosion in fluvial catchments in the Himalaya, and they show little variability between long-term and present-day erosion rates (Lenard et al., 2020; Vance et al., 2003). Furthermore, large basins exhibit broad similarity in sediment discharge recorded by the gauge-derived and cosmogenic radionuclide-derived sediment loads from global compilations of literature data (Covault et al., 2013; Wittmann et al., 2020). This suggests that erosion rates across different timescales can be comparable in active orogens such as the Ayeyarwady catchment. For instance, in the adjacent Ganges-Brahmaputra (983.9 ± 209 vs. 1037 Mt/a) and Mekong (54.8 ± 6.4 vs. 78 Mt/a) systems—located west and east of the Ayeyarwady, respectively—

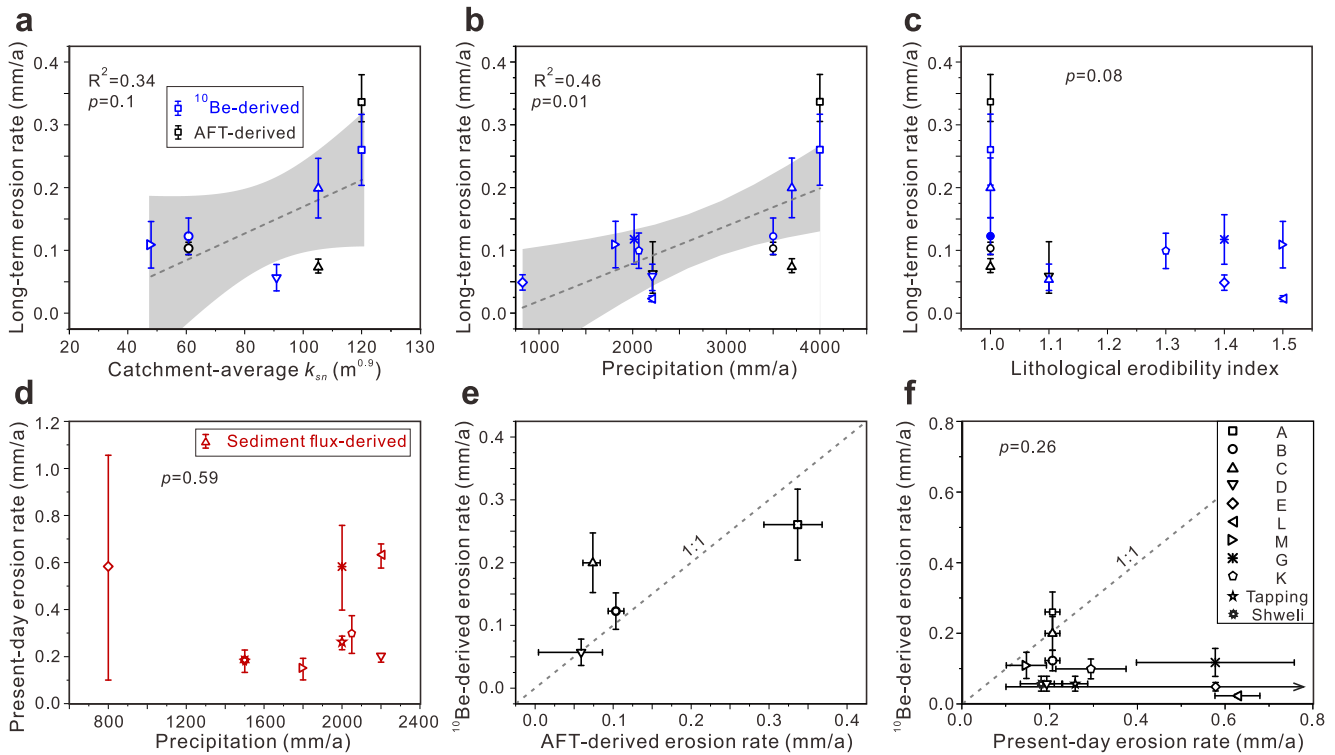


Figure 7. Correlations between erosion rates at different timescales and their potential controls with 95% confidence band in gray. (a–b) Long-term natural erosion rates versus catchment-average k_{sn} and precipitation. (c) Long-term natural erosion rates versus lithological erodibility (rock erodibility index from Moosdorf et al., 2018). (d) Present-day erosion rate versus precipitation. (e) ^{10}Be -derived versus AFT-derived erosion rates. (f) ^{10}Be -derived versus present-day erosion rates (capital letters in key denote sample sites as per Figure 1b).

cosmogenic and gauge-derived sediment loads show close agreement (Wittmann et al., 2020). Thus, we consider that the variations we record are not an artifact of the different measuring approaches we use for different timescales.

This inversion in the scale of erosion between the Chindwin and Upper Ayeyarwady catchments cannot be ascribed to climatic factors, because present-day erosion rates do not significantly correlate with precipitation ($p = 0.59$, Figure 7d). Moreover, the source-rock lithologies likely remained broadly unchanged over this relatively short timescale, indicating that lithological differences are not responsible for the sharp increase in present-day sediment fluxes of the Chindwin River. Whilst we cannot totally rule out the potential effects of neotectonics in this poorly mapped region, we argue below that anthropogenic influence is a major contributing factor.

5.4. Accelerated Erosion by Anthropogenic Activities

Previous research has shown how modern sediment yields may increase by one or even two orders of magnitude relative to long-term cosmogenic-derived sediment yields if river catchments are affected by profound changes in land use (Hewawasam et al., 2003; Vanacker et al., 2007). This appears to be the case for the Ayeyarwady catchment, and here we emphasize that anthropogenic activities represent an important factor driving the sharp recent acceleration in sediment production.

First, alluvial mining, which is affecting no less than one-third of the river length in Myanmar (Figure 6c, Dethier et al., 2023; Shrestha et al., 2020). Satellite imagery reveals that mining areas in Myanmar have expanded rapidly over the last 13 years (Connette et al., 2016). Landsat data from 1985 to 2020 reveal that mining has significantly increased suspended sediment concentrations (SSC) in 23 trunk and tributary rivers of the Chindwin and Upper Ayeyarwady (Dethier et al., 2023; Figure S1 in Supporting Information S1). Notably, SSC in the Chindwin River has risen more than tenfold, with the Uyu River—an eastern tributary—experiencing increases of over two orders of magnitude relative to pre-mining levels (Figure 8; Figures S2–S3 in Supporting Information S1). Sediment

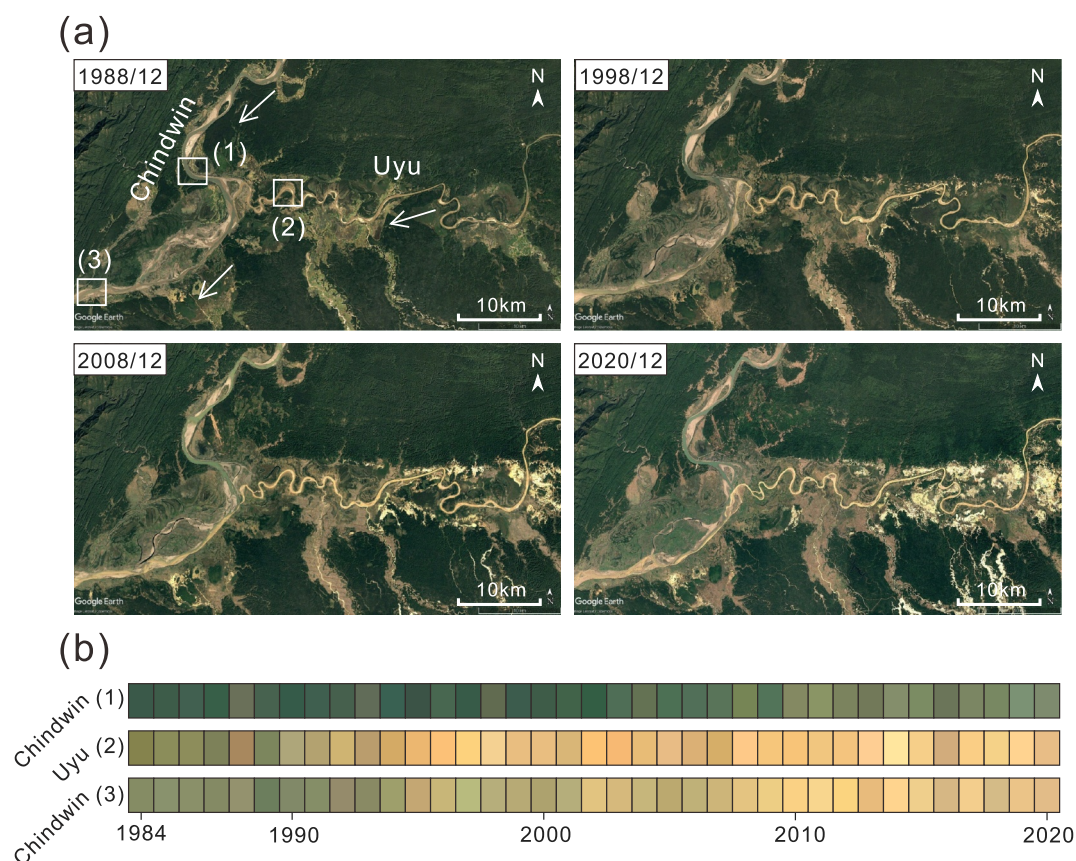


Figure 8. Expansion of river mining activities has led to increased suspended sediment concentrations in the Chindwin and Uyu rivers. (a) Representative images from Google Earth Pro from 1988, 1998, 2008 and 2020 show expansion of river mining activities in the Uyu River drainage. White arrows show the river direction. White boxes refer to location of data shown in (b) (b) Average river true color obtained through Landsat imagery (Landsat 5 and Landsat 7) from 1984 to 2020 in December using the average red-green-blue (RGB) reflectance method (Dethier et al., 2022). The color gradient, ranging from blue to yellow, indicates increasing suspended sediment concentration. The bar numbers in (b) correspond to the locations shown in the first image of (a).

fluxes and present-day erosion rates correlate strongly with the proportion of land impacted by mining (Figures 9a and 9b). Alluvial mining is most widespread in the Upper Chindwin catchment, which also shows the greatest increase in sediment discharge. Mining-affected areas in the Upper Chindwin (16%, ~1869 km²) far exceeds those in the Upper Ayeyarwady (1%, ~74 km²); correspondingly, present-day erosion rates are three times higher in the Upper Chindwin River (0.63 ± 0.05 mm/a) than in the Upper Ayeyarwady (0.19 ± 0.02 mm/a) (Figures 6c, 9a-9b).

Second, additional anthropogenic factors likely also contributed to enhanced erosion rates. Forest loss has been particularly severe in the Lower Ayeyarwady and delta regions due to cropland expansion, with mean annual deforestation rates reaching 1%–2% (Table 1, Figures S4d in Supporting Information S1). In the Upper Chindwin and Upper Ayeyarwady catchments, forest cover has declined by 21% and 23%, respectively (Table 1; Figures S4a–S4d in Supporting Information S1), potentially contributing to the observed sediment flux increases in a similar trend. However, the increase in sediment flux in the Upper Chindwin (~30-fold) far exceeds that in the Upper Ayeyarwady (~3-fold), indicating that deforestation alone cannot account for the difference. In the Chindwin, mining activity—often linked to deforestation itself—likely plays a dominant role (Figures S4d, S5d–S5e in Supporting Information S1; McGinn et al., 2021). Other land-use changes, such as settlement expansion, have also contributed to landscape disturbance. Conversely, agricultural land use likely does not explain the increase in Chindwin sediment fluxes, as the cultivated area decreased by ~20% between 1999 and 2019 (Table 1). Agriculture is more concentrated in the central and lower plains, including the Mu River basin and Lower Ayeyarwady (Li et al., 2024), and may instead contribute to sediment increases there.

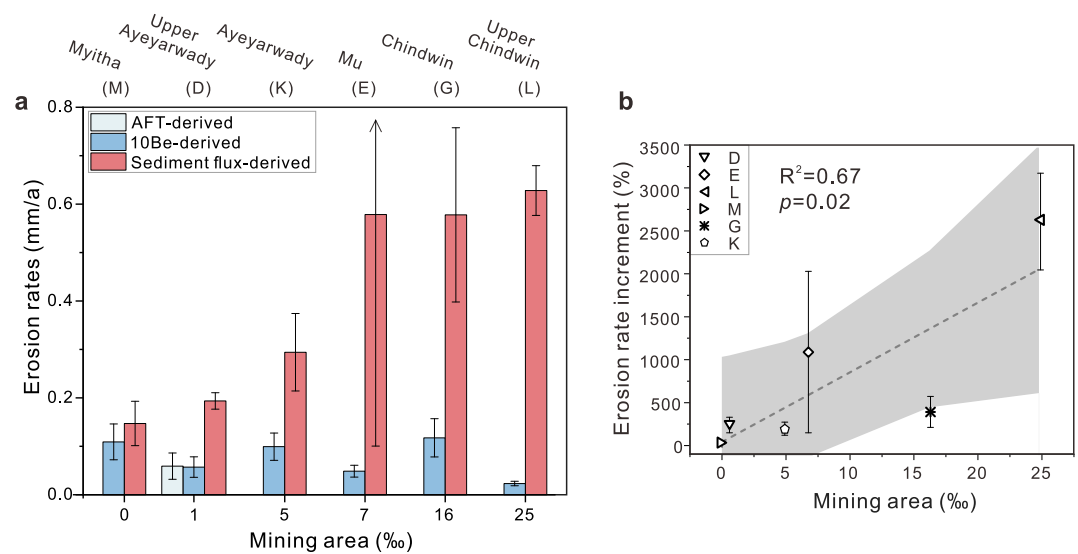


Figure 9. Erosion rates increment positively correlated with the proportion of mining area. (a) Present-day erosion rates increase with the mining area proportion expanding. (b) Erosion rates increment positively correlated with the mining area proportion increasing. Erosion rates increment = $100 \times (\text{present-day erosion rates} - \text{long-term erosion rates}) / \text{long-term erosion rates}$.

Third, climatic factors such as increased precipitation and temperature—linked, at least in part, to 20th-century global warming—may further enhance erosion in all Ayeyarwady sub-catchments. Between 1981 and 2015, both parameters rose across the Ayeyarwady catchment (Sein et al., 2018), while Southeast Asia experienced more frequent extreme monsoon floods (Loo et al., 2015). These climatic trends may have amplified sediment fluxes in both the Upper Ayeyarwady and Chindwin.

Other anthropogenic influences appear limited. Large dams are absent from the main Ayeyarwady, and only small dams exist on select tributaries, suggesting minimal hydrological disruption from damming (Schmitt et al., 2021).

In summary, alluvial mining is the primary driver of elevated sediment fluxes in the Upper Chindwin, with deforestation providing additional impact. In the Upper Ayeyarwady, both deforestation and mining contribute to increased sediment yields. In contrast, cropland expansion and associated deforestation are the main factors behind increased sediment fluxes in the Lower Ayeyarwady. Intensifying precipitation and more frequent monsoon floods may further augment sediment flux across all sub-catchments. The rapid acceleration in anthropogenic-related erosional processes greatly increased the concentration of suspended sediment (Dethier

Table 1
Ayeyarwady Catchment Land Use and Land Cover Changes

Land type	Catchment	Previous area (km ²)	Recent area (km ²)	Changes (%)	Period	References
Forestry Coverage	Uyu			−8.90	1999–2019	McGinn et al. (2021)
	Upper Chindwin	636,000	500,000	−21.38	1988–2017	Yang et al. (2019)
	Lower Chindwin			4.60	1999–2019	McGinn et al. (2021)
	Chindwin	8,804,521	8,576,294	−2.59	1999–2019	McGinn et al. (2021)
	Upper Ayeyarwady	210,700	162,400	−22.92	1988–2017	Yang et al. (2019)
	Lower Ayeyarwady	54,000	20,100	−62.78	1988–2017	Yang et al. (2019)
	Total Myanmar	391,705	381,648	−2.57	1990–2020	Li et al. (2024)
Agriculture Coverage	Uyu			1.00	1999–2019	McGinn et al. (2021)
	Lower Chindwin			−10.40	1999–2019	McGinn et al. (2021)
	Chindwin	1,229,445	985,161	−19.87	1999–2019	McGinn et al. (2021)
	Total Myanmar	152,687	153,117	0.28	1990–2020	Li et al. (2024)

et al., 2023), resulting in degraded water quality and threats to the life cycles of riverine and riparian flora and fauna (Azevedo-Santos et al., 2021; Keovilignavong, 2019) and to natural equilibria as far as the Ayeyarwady Delta (Chen et al., 2020).

6. Conclusions

Long-term natural erosion rates calculated from apatite fission-track ages and ^{10}Be concentration in quartz grains were much higher in the Upper Ayeyarwady (0.06–0.34 mm/a) than in the Upper Chindwin (0.02 ± 0.005 mm/a) derived by ^{10}Be and controlled by tectonic forcing and climate. Gauged sediment fluxes testify to a drastically different modern scenario. Present-day erosion rates have increased by more than an order of magnitude in the Upper Chindwin and Mu catchments, enough to reverse erosion patterns: despite a three-fold increase in the Upper Ayeyarwady, erosion is now notably faster in the Upper Chindwin (0.63 ± 0.05 mm/a) than in the Upper Ayeyarwady (0.19 ± 0.02 mm/a). Such a recent drastic change in erosion patterns underscores a profound impact of anthropogenic activities, especially extensive alluvial mining for jade and gold in the Upper Chindwin catchment. The expansion of land use related deforestation, and global warming in the 20th century increasing in precipitation and extreme flooding events likely also contributed to increased sediment fluxes in both the Chindwin and Upper Ayeyarwady catchments. Accelerated erosion and consequently increased sediment yield by anthropogenic activities have reduced water quality and changed the natural equilibrium in the Ayeyarwady delta.

Data Availability Statement

Data sets (Tables S1–S9 in Supporting Information S2) and Supporting Information S1 from this research are provided in the Figshare repository, which are publicly available via <https://doi.org/10.6084/m9.figshare.27747153.v9> (Dong et al., 2025).

Acknowledgments

We are deeply grateful to the Editor Mikael Attal, to three anonymous reviewers, and to the handling Associate Editor for their constructive comments and helpful suggestions. We thank Xu Ying of Nanjing Hongchuang Geological Service Co., Ltd. for apatite separation, and Yizhou Wang and Edward R. Sobel for help with detrital AFT inversion modeling and data interpretation. We are also grateful to Fei Liu and Nyanmin Naing for sampling in the field, and to Abaz Alimanovic and Keith Fifield for ^{10}Be cosmogenic analysis. This study was financially supported by the Second Tibetan Plateau Scientific Expedition and Research Program (STEP, Grant Number 2019QZKK0204) and National Natural Science Foundation of China (Number 42272111).

References

- Allen, R., Najman, Y., Carter, A., Parrish, R., Bickle, M., Paul, M., et al. (2008). Provenance of the Tertiary sedimentary rocks of the Indo-Burman Ranges, Burma (Myanmar): Burman arc or Himalayan-derived? *Journal of the Geological Society*, *165*(6), 1045–1057. <https://doi.org/10.1144/0016-76492007-143>
- Andò, S., & Garzanti, E. (2014). *Raman spectroscopy in heavy-mineral studies* (Vol. 386, pp. 395–412). Geological Society, London, Special Publications. <https://doi.org/10.1144/SP386.2>
- Avdeev, B., Niemi, N. A., & Clark, M. K. (2011). Doing more with less: Bayesian estimation of erosion models with detrital thermochronometric data. *Earth and Planetary Science Letters*, *305*(3–4), 385–395. <https://doi.org/10.1016/j.epsl.2011.03.020>
- Azevedo-Santos, V. M., Arcifa, M. S., Brito, M. F. G., Agostinho, A. A., Hughes, R. M., Vitule, J. R. S., et al. (2021). Negative impacts of mining on Neotropical freshwater fishes. *Neotropical Ichthyology*, *19*(3). <https://doi.org/10.1590/1982-0224-2021-0001>
- Barbarand, J., Carter, A., Wood, I., & Hurford, T. (2003). Compositional and structural control of fission-track annealing in apatite. *Chemical Geology*, *198*(1–2), 107–137. [https://doi.org/10.1016/S0009-2541\(02\)00424-2](https://doi.org/10.1016/S0009-2541(02)00424-2)
- Baronas, J. J., Stevenson, E. I., Hackney, C. R., Darby, S. E., Bickle, M. J., Hilton, R. G., et al. (2020). Integrating suspended sediment flux in large alluvial river channels: Application of a synoptic rouse-based model to the Irrawaddy and Salween Rivers. *Journal of Geophysical Research: Earth Surface*, *125*(9), e2020JF005554. <https://doi.org/10.1029/2020JF005554>
- Bender, F. (1983). *Geology of Burma*. Bonaerae.
- Bertrand, G., Rangin, C., Maluski, H., Bellon, H., & Party, G. S. (2001). Diachronous cooling along the Mogok Metamorphic Belt (Shan scarp, Myanmar): The trace of the northward migration of the Indian syntaxis. *Journal of Asian Earth Sciences*, *19*(5), 649–659.
- Best, J. (2018). Anthropogenic stresses on the world's big rivers. *Nature Geoscience*, *12*(1), 7–21. <https://doi.org/10.1038/s41561-018-0262-x>
- Betka, P. M., Seeber, L., Thomson, S. N., Steckler, M. S., Sincavage, R., & Zoramthara, C. (2018). Slip-partitioning above a shallow, weak decollement beneath the Indo-Burman accretionary prism. *Earth and Planetary Science Letters*, *503*, 17–28. <https://doi.org/10.1016/j.epsl.2018.09.003>
- Brunschweiler, R. O. (1966). On the geology of the Indoburman ranges. *Journal of the Geological Society of Australia*, *13*(1), 137–194. <https://doi.org/10.1080/00167616608728608>
- Burma Earth Sciences Research Division. (1977a). *Geological map of the socialist Re-public of the Union of Burma, 1:1000000*. Security Printing Works.
- Burma Earth Sciences Research Division. (1977b). *Geological map of the socialist Re-public of the Union of Burma, 1:1,500,000*. Security Printing Works.
- Chen, D., Li, X., Saito, Y., Liu, J. P., Duan, Y., Liu, S. a., & Zhang, L. (2020). Recent evolution of the Irrawaddy (Ayeyarwady) Delta and the impacts of anthropogenic activities: A review and remote sensing survey. *Geomorphology*, *365*, 107231. <https://doi.org/10.1016/j.geomorph.2020.107231>
- Chinese Hydrological Yearbooks. (2021). *Ministry of Water Conservancy and Electric Power, People's Republic of China (MWCEPC)*. Chinese Hydrological Yearbooks. (in Chinese).
- Codilean, A. T. (2006). Calculation of the cosmogenic nuclide production topographic shielding scaling factor for large areas using DEMs. *Earth Surface Processes and Landforms*, *31*(6), 785–794. <https://doi.org/10.1002/esp.1336>
- Cohen, S., Syvitski, J., Ashley, T., Lammers, R., Fekete, B., & Li, H. Y. (2022). Spatial trends and drivers of bedload and suspended sediment fluxes in global Rivers. *Water Resources Research*, *58*(6), e2021WR031583. <https://doi.org/10.1029/2021WR031583>
- Connette, K. L., Connette, G., Bernd, A., Phyo, P., Aung, K., Tun, Y., et al. (2016). Assessment of mining extent and expansion in Myanmar based on freely-available satellite imagery. *Remote Sensing*, *8*(11), 912. <https://doi.org/10.3390/rs8110912>

- Covault, J. A., Craddock, W. H., Romans, B. W., Fildani, A., & Gosai, M. (2013). Spatial and temporal variations in landscape evolution: Historic and longer-term sediment flux through global catchments. *The Journal of Geology*, *121*(1), 35–56. <https://doi.org/10.1086/668680>
- Dang, T. H., Coynel, A., Orange, D., Blanc, G., Etcheber, H., & Le, L. A. (2010). Long-term monitoring (1960–2008) of the river-sediment transport in the red river watershed (Vietnam): Temporal variability and dam-reservoir impact. *Science of The Total Environment*, *408*(20), 4654–4664. <https://doi.org/10.1016/j.scitotenv.2010.07.007>
- Dethier, E. N., Renshaw, C. E., & Magilligan, F. J. (2022). Rapid changes to global river suspended sediment flux by humans. *Science*, *376*(6600), 1447–1452. <https://doi.org/10.1126/science.abn798>
- Dethier, E. N., Silman, M., Leiva, J. D., Alqahtani, S., Fernandez, L. E., Pauca, P., et al. (2023). A global rise in alluvial mining increases sediment load in tropical rivers. *Nature*, *620*(7975), 787–793. <https://doi.org/10.1038/s41586-023-06309-9>
- Dong, X., Hu, X., Li, G., Garzanti, E., Najman, Y., Liang, W., et al. (2025). Dataset for accelerated erosion and sediment fluxes by anthropogenic mining activities in the Irrawaddy River [Dataset]. *figshare*. <https://doi.org/10.6084/m9.figshare.27747153.v9>
- Duvall, A. R., Clark, M. K., Avdeev, B., Farley, K. A., & Chen, Z. (2012). Widespread late Cenozoic increase in erosion rates across the interior of eastern Tibet constrained by detrital low-temperature thermochronometry. *Tectonics*, *31*(3), TC3014. <https://doi.org/10.1029/2011TC002969>
- Furuichi, T., Win, Z., & Wasson, R. J. (2009). Discharge and suspended sediment transport in the Ayeyarwady River, Myanmar: Centennial and decadal changes. *Hydrological Processes*, *23*(11), 1631–1641. <https://doi.org/10.1002/hyp.7295>
- Gallagher, K., Brown, R. W., & Johnson, C. (1998). Fission track analysis and its applications to geological problems. *Annual Review of Earth and Planetary Sciences*, *26*(1), 519–572. <https://doi.org/10.1146/annurev.earth.26.1.519>
- Garzanti, E. (2019). Petrographic classification of sand and sandstone. *Earth-Science Reviews*, *192*, 545–563. <https://doi.org/10.1016/j.earscirev.2018.12.014>
- Garzanti, E., & Andò, S. (2007). Heavy-mineral concentration in modern sands: Implications for provenance interpretation. In M. Mange & D. Wright (Eds.), *Heavy minerals in use, developments in sedimentology series* (Vol. 58, pp. 517–545). [https://doi.org/10.1016/S0070-4571\(07\)58020-9](https://doi.org/10.1016/S0070-4571(07)58020-9)
- Garzanti, E., & Andò, S. (2019). Heavy minerals for junior woodchucks. *Minerals*, *9*(3), 148. <https://doi.org/10.3390/min9030148>
- Garzanti, E., Resentini, A., Vezzoli, G., Andò, S., Malusà, M., & Padoan, M. (2012). Forward compositional modelling of Alpine orogenic sediments. *Sedimentary Geology*, *280*, 149–164. <https://doi.org/10.1016/j.sedgeo.2012.03.012>
- Garzanti, E., Wang, J.-G., Vezzoli, G., & Limonta, M. (2016). Tracing provenance and sediment fluxes in the Irrawaddy River basin (Myanmar). *Chemical Geology*, *440*, 73–90. <https://doi.org/10.1016/j.chemgeo.2016.06.010>
- Gleadow, A. J. W., Gleadow, S. J., Belton, D. X., Kohn, B. P., Krochmal, M. S., & Brown, R. W. (2009). *Coincidence mapping - A key strategy for the automatic counting of fission tracks in natural minerals* (Vol. 324, pp. 25–36). Geological Society, London, Special Publications. <https://doi.org/10.1144/SP324.2>
- Gordon, R. (1885). The irawadi river. *Proceedings of the royal geographical society and monthly record of geography*, *7*(5), 292–331. <https://doi.org/10.2307/1800379>
- Hasebe, N., Barbarand, J., Jarvis, K., Carter, A., & Hurford, A. J. (2004). Apatite fission-track chronometry using laser ablation ICP-MS. *Chemical Geology*, *207*(3–4), 135–145. <https://doi.org/10.1016/j.chemgeo.2004.01.007>
- Hewawasam, T., Blanckenburg, F. v., Schaller, M., & Kubik, P. (2003). Increase of human over natural erosion rates in tropical highlands constrained by cosmogenic nuclides. *Geology*, *31*(7), 597–600. [https://doi.org/10.1130/0091-7613\(2003\)031<0597:IOHONE>2.0.CO;2](https://doi.org/10.1130/0091-7613(2003)031<0597:IOHONE>2.0.CO;2)
- Inam, A., Clift, P., Giosan, L., Tabrez, A., Tahir, M., Rabbani, M. M., & Danish, M. (2007). The geographic, geological and oceanographic setting of the Indus River. *Large Rivers: Geomorphology and Management*, *1*, 333–346. <https://doi.org/10.1002/9781119412632.ch17>
- Ingersoll, R. V., Bullard, T. F., Ford, R. L., Grimm, J. P., Pickle, J. D., & Sares, S. W. (1984). The effect of grain size on detrital modes: A test of the Gazzi–Dickinson point-counting method. *Journal of Sedimentary Petrology*, *54*, 103–116. <https://doi.org/10.1306/212F83B9-2B24-11D7-8648000102C1865D>
- International Finance Corporation (IFC). (2017). Baseline assessment report: Geomorphic and sediment transport. In *Strategic environmental assessment of the hydropower sector in Myanmar* (pp. 1–44).
- Islam, M. R., Begum, S. F., Yamaguchi, Y., & Ogawa, K. (1999). The Ganges and Brahmaputra rivers in Bangladesh: Basin denudation and sedimentation. *Hydrological Processes*, *13*(17), 2907–2923. [https://doi.org/10.1002/\(SICI\)1099-1085\(19991215\)13:17<2907::AID-HYP906>3.0.CO;2-E](https://doi.org/10.1002/(SICI)1099-1085(19991215)13:17<2907::AID-HYP906>3.0.CO;2-E)
- Keovilignavong, O. (2019). Mining governance dilemma and impacts: A case of gold mining in Phu-Hae, Lao PDR. *Resources Policy*, *61*, 141–150. <https://doi.org/10.1016/j.resourpol.2019.02.002>
- Kuiper, N. H. (1962). Tests concerning random points on a circle. *Proceedings of the Koninklijke Nederlandse Akademie van Wetenschappen Series A*, *63*, 38–47. [https://doi.org/10.1016/s1385-7258\(60\)50006-0](https://doi.org/10.1016/s1385-7258(60)50006-0)
- Kyaw Linn, O., Khin, Z., Meffre, S., Myitta, Day Wa, A., & Lai, C.-K. (2015). Provenance of the Eocene sandstones in the southern Chindwin Basin, Myanmar: Implications for the unroofing history of the Cretaceous–Eocene magmatic arc. *Journal of Asian Earth Sciences*, *107*, 172–194. <https://doi.org/10.1016/j.jseas.2015.04.029>
- Lal, D. (1991). Cosmic ray labeling of erosion surfaces: In situ nuclide production rates and erosion models. *Earth and Planetary Science Letters*, *104*(2–4), 424–439. [https://doi.org/10.1016/0012-821X\(91\)90220-C](https://doi.org/10.1016/0012-821X(91)90220-C)
- Lei, Y. L., Ji, J. Q., Gong, D. H., Zhong, D. L., Wang, X. S., Zhang, J., & Wang, X. M. (2006). Thermal and denudational history of granitoid batholith recorded by apatite fission track in the Dulong River region in northwestern Yunnan, since Late Miocene. *Acta Petrologica Sinica*, *22*(4), 938–948. [1000-0569/2006/022\(04\)-0938-48 http://www.yssxb.ac.cn/en/article/id/aps_20060499](http://www.yssxb.ac.cn/en/article/id/aps_20060499)
- Lenard, S. J. P., Lavé, J., France-Lanord, C., Aumaître, G., Bourlès, D. L., & Keddadouche, K. (2020). Steady erosion rates in the Himalayas through late Cenozoic climatic changes. *Nature Geoscience*, *13*(6), 448–452. <https://doi.org/10.1038/s41561-020-0585-2>
- Li, R., Li, C., Hou, D., Xing, H., & Zhu, A. X. (2024). Dynamics in land cover and landscape patterns of Myanmar: A three-decade perspective (1990–2020). *Land*, *13*(12), 2212. <https://doi.org/10.3390/land1312212>
- Licht, A., Win, Z., Westerweel, J., Cogné, N., Morley, C. K., Chantraprasert, S., et al. (2020). Magmatic history of central Myanmar and implications for the evolution of the Burma Terrane. *Gondwana Research*, *87*, 303–319. <https://doi.org/10.1016/j.gr.2020.06.016>
- Lindert, P. H. (2000). Shifting ground: The changing agricultural soils of China and Indonesia. *Journal of Asian Studies*, *60*, 824–825. <https://doi.org/10.7551/mitpress/6212.001.0001>
- Loo, Y. Y., Billa, L., & Singh, A. (2015). Effect of climate change on seasonal monsoon in Asia and its impact on the variability of monsoon rainfall in Southeast Asia. *Geoscience Frontiers*, *6*(6), 817–823. <https://doi.org/10.1016/j.gsf.2014.02.009>
- Lupker, M., Blard, P.-H., Lavé, J., France-Lanord, C., Leanni, L., Puchol, N., et al. (2012). ¹⁰Be-derived Himalayan denudation rates and sediment budgets in the Ganga basin. *Earth and Planetary Science Letters*, *333*, 146–156. <https://doi.org/10.1016/j.epsl.2012.04.020>

- Lupker, M., Lavé, J., France-Lanord, C., Christl, M., Bourlès, D., Carcaillet, J., et al. (2017). ¹⁰Be systematics in the Tsangpo-Brahmaputra catchment: The cosmogenic nuclide legacy of the eastern Himalayan syntaxis. *Earth Surface Dynamics*, 5(3), 429–449. <https://doi.org/10.5194/esurf-5-429-2017>
- Maus, V., Giljum, S., da Silva, D. M., Gutschhofer, J., da Rosa, R. P., Luckeneder, S., et al. (2022). An update on global mining land use. *Scientific Data*, 9(1), 433. <https://doi.org/10.1038/s41597-022-01547-4>
- McGinn, A. J., Wagner, P. D., Htike, H., Kyu, K. K., & Fohrer, N. (2021). Twenty years of change: Land and water resources in the Chindwin catchment, Myanmar between 1999 and 2019. *The Science of the Total Environment*, 798, 148766. <https://doi.org/10.1016/j.scitotenv.2021.148766>
- Mitchell, A. H. G. (1993). Cretaceous-Cenozoic tectonic events in the western Myanmar(Burma)-Assam region. *Journal of the Geological Society*, 150(6), 1089–1102. <https://doi.org/10.1144/gsjgs.150.6.1089>
- Mitchell, A. H. G., Chung, S.-L., Thura, O., Lin, T.-S., & Hung, C.-H. (2012). Zircon U-Pb ages in Myanmar: Magmatic-metamorphic events and the closure of a Neotethys ocean? *Journal of Asian Earth Sciences*, 56, 1–23. <https://doi.org/10.1016/j.jseas.2012.04.019>
- Moosdorf, N., Cohen, S., & von Hagke, C. (2018). A global erodibility index to represent sediment production potential of different rock types. *Applied Geography*, 101, 36–44. <https://doi.org/10.1016/j.apgeog.2018.10.010>
- Naing, T. T., Bussien, D. A., Winkler, W. H., Nold, M., & Von Quadt, A. (2014). Provenance study on Eocene-Miocene sandstones of the Rakhine Coastal Belt, Indo-Burman Ranges of Myanmar: Geodynamic implications. *Geological Society, London, Special Publications*, 386(1), 195–216. <https://doi.org/10.1144/SP386.10>
- Najman, Y., Sobel, E. R., Millar, I., Luan, X., Zapata, S., Garzanti, E., et al. (2022). The timing of collision between Asia and the West Burma terrane, and the development of the indo-burman ranges. *Tectonics*, 41(7), e2021TC007057. <https://doi.org/10.1029/2021TC007057>
- Najman, Y., Sobel, E. R., Millar, I., Stockli, D. F., Govin, G., Lisker, F., et al. (2020). The exhumation of the Indo-Burman Ranges, Myanmar. *Earth and Planetary Science Letters*, 530, 115948. <https://doi.org/10.1016/j.epsl.2019.115948>
- Robinson, R. A. J., Bird, M. I., Oo, N. W., Hoey, T. B., Aye, M. M., Higgitt, D. L., et al. (2007). The Irrawaddy River sediment flux to the Indian Ocean: The original nineteenth-century data revisited. *The Journal of Geology*, 115(6), 629–640. <https://doi.org/10.1086/521607>
- Ruhl, K. W., & Hodges, K. V. (2005). The use of detrital mineral cooling ages to evaluate steady state assumptions in active orogens: An example from the central Nepalese Himalaya. *Tectonics*, 24(4), TC4015. <https://doi.org/10.1029/2004TC001712>
- Schaefer, J. M., Codilean, A. T., Willenbring, J. K., Lu, Z.-T., Keisling, B., Fülöp, R.-H., & Val, P. (2022). Cosmogenic nuclide techniques. *Nature Reviews Methods Primers*, 2(1), 18. <https://doi.org/10.1038/s43586-022-00096-9>
- Schmitt, R. J. P., Kittner, N., Kondolf, G. M., & Kammen, D. M. (2021). Joint strategic energy and river basin planning to reduce dam impacts on rivers in Myanmar. *Environmental Research Letters*, 16(5), 054054. <https://doi.org/10.1088/1748-9326/abe329>
- Sein, K. K., Chidthaisong, A., & Oo, K. L. (2018). Observed trends and changes in temperature and precipitation extreme indices over Myanmar. *Atmosphere*, 9(12), 477. <https://doi.org/10.3390/atmos9120477>
- Shrestha, S., Gunawardana, S. K., Piman, T., & Babel, M. S. (2020). Assessment of the impact of climate change and mining activities on streamflow and selected metal's loading in the Chindwin River, Myanmar. *Environmental Research*, 181, 108942. <https://doi.org/10.1016/j.envres.2019.108942>
- Sirisena, T. A. J. G., Maskey, S., Bamanawala, J., & Ranasinghe, R. (2021). Climate change and reservoir impacts on 21st-Century streamflow and fluvial sediment loads in the Irrawaddy River, Myanmar. *Frontiers in Earth Science*, 9. <https://doi.org/10.3389/feart.2021.644527>
- Sirisena, T. A. J. G., Maskey, S., Ranasinghe, R., & Babel, M. S. (2018). Effects of different precipitation inputs on streamflow simulation in the Irrawaddy River Basin, Myanmar. *Journal of Hydrology: Regional Studies*, 19, 265–278. <https://doi.org/10.1016/j.ejrh.2018.10.005>
- Sok, T., Oeung, C., Kaing, V., Sauvage, S., Kondolf, G. M., & Sánchez-Pérez, J. M. (2021). Assessment of suspended sediment load variability in the Tonle Sap and Lower Mekong Rivers, Cambodia. *Catena*, 202, 105291. <https://doi.org/10.1016/j.catena.2021.105291>
- Stone, J. O. (2000). Air pressure and cosmogenic isotope production. *Journal of Geophysical Research*, 105(B10), 23753–23759. <https://doi.org/10.1029/2000JB900181>
- Suzuki, H., Maung, M., Aung, A. K., & Takai, M. (2004). Jurassic radiolaria from chert pebbles of the Eocene Pondaung Formation, central Myanmar. *Neues Jahrbuch für Geologie und Paläontologie - Abhandlungen*, 231(3), 369–393. <https://doi.org/10.1127/njgpa/231/2004/369>
- Syvitski, J. P., & Kettner, A. (2011). Sediment flux and the Anthropocene. *Philosophical Transactions of the Royal Society A*, 369(1938), 957–975. <https://doi.org/10.1098/rsta.2010.0329>
- Vanacker, V., von Blanckenburg, F., Govers, G., Molina, A., Poesen, J., Deckers, J., & Kubik, P. (2007). Restoring dense vegetation can slow mountain erosion to near natural benchmark levels. *Geology*, 35(4), 303–306. <https://doi.org/10.1130/G23109A.1>
- Vance, D., Bickle, M., Ivy-Ochs, S., & Kubik, P. W. (2003). Erosion and exhumation in the Himalaya from cosmogenic isotope inventories of river sediments. *Earth and Planetary Science Letters*, 206(3–4), 273–288. [https://doi.org/10.1016/S0012-821X\(02\)01102-0](https://doi.org/10.1016/S0012-821X(02)01102-0)
- Vermeesch, P. (2007a). CosmoCalc: An Excel add-in for cosmogenic nuclide calculations. *Geochemistry, Geophysics, Geosystems*, 8, Q08003. <https://doi.org/10.1029/2006GC001530>
- Vermeesch, P. (2007b). Quantitative geomorphology of the White Mountains (California) using detrital apatite fission track thermochronology. *Journal of Geophysical Research*, 112(F3), F03004. <https://doi.org/10.1029/2006JF000671>
- Vermeesch, P. (2012). On the visualisation of detrital age distributions. *Chemical Geology*, 312, 190–194. <https://doi.org/10.1016/j.chemgeo.2012.04.021>
- Wang, H., Saito, Y., Zhang, Y., Bi, N., Sun, X., & Yang, Z. (2011). Recent changes of sediment flux to the western Pacific Ocean from major rivers in east and southeast Asia. *Earth-Science Reviews*, 108(1–2), 80–100. <https://doi.org/10.1016/j.earscirev.2011.06.003>
- Wittmann, H., Oelze, M., Gaillardet, J., Garzanti, E., & von Blanckenburg, F. (2020). A global rate of denudation from cosmogenic nuclides in the Earth's largest rivers. *Earth-Science Reviews*, 204, 103147. <https://doi.org/10.1016/j.earscirev.2020.103147>
- Yang, R., Luo, Y., Yang, K., Hong, L., & Zhou, X. (2019). Analysis of forest deforestation and its driving factors in Myanmar from 1988 to 2017. *Sustainability*, 11(11), 3047. <https://doi.org/10.3390/su11113047>
- Ye, Y., Wu, L., Cowgill, E., Tian, Y., Lin, X., Xiao, A., & Chen, H. (2022). Long-lagged (~19 Myr) response of accelerated river incision to rock uplift on the northern margin of the Tibetan Plateau. *Earth and Planetary Science Letters*, 591, 117608. <https://doi.org/10.1016/j.epsl.2022.117608>
- Zaw, K., Swe, W., Barber, A. J., Crow, M. J., & Nwe, Y.-Y. (2017). Introduction to the geology of Myanmar. *Geological Society, London, Memoirs*, 48(1), 1–17. <https://doi.org/10.1144/M48.1>
- Zhang, H., Kirby, E., Pitlick, J., Anderson, R. S., & Zhang, P. (2017). Characterizing the transient geomorphic response to base-level fall in the northeastern Tibetan Plateau. *Journal of Geophysical Research: Earth Surface*, 122(2), 546–572. <https://doi.org/10.1002/2015JF003715>

Zhuang, G., Najman, Y., Tian, Y., Carter, A., Gemignani, L., Wijbrans, J., et al. (2018). Insights into the evolution of the Hindu Kush–Kohistan–Karakoram from modern river sand detrital geo- and thermochronological studies. *Journal of the Geological Society*, *175*(6), 934–948. <https://doi.org/10.1144/jgs2018-007>

References From the Supporting Information

- Aitchison, J. (1982). The statistical analysis of compositional data. *Journal of the Royal Statistical Society - Series B: Statistical Methodology*, *44*(2), 139–160. <https://doi.org/10.1111/j.2517-6161.1982.tb01195.x>
- Clubb, F. J., Mudd, S. M., Schildgen, T. F., van der Beek, P. A., Devrani, R., & Sinclair, H. D. (2023). Himalayan valley-floor widths controlled by tectonically driven exhumation. *Nature Geoscience*, *16*(8), 739–746. <https://doi.org/10.1038/s41561-023-01238-8>
- Flint, J. J. (1974). Stream gradient as a function of order, magnitude, and discharge. *Water Resources Research*, *10*(5), 969–973. <https://doi.org/10.1029/WR010i005p00969>
- Gallen, S. F., & Wegmann, K. W. (2017). River profile response to normal fault growth and linkage: An example from the Hellenic forearc of south-central Crete, Greece. *Earth Surface Dynamics*, *5*(1), 161–186. <https://doi.org/10.5194/esurf-5-161-2017>
- Garzanti, E., He, J., Barbarano, M., Resentini, A., Li, C., Yang, L., et al. (2021). Provenance versus weathering control on sediment composition in tropical monsoonal climate (south China) - 2. Sand petrology and heavy minerals. *Chemical Geology*, *564*, 119997. <https://doi.org/10.1016/j.chemgeo.2020.119997>
- Martín-Fernández, J. A., C. B.-V. P. V. P.-G., & Pawlowsky-Glahn, V. (2003). Dealing with zeros and missing values in compositional data sets using nonparametric imputation. *Mathematical Geology*, *35*(3), 253–278. <https://doi.org/10.1023/A:1023866030544>
- Kirby, E., & Whipple, K. X. (2012). Expression of active tectonics in erosional landscapes. *Journal of Structural Geology*, *44*, 54–75. <https://doi.org/10.1016/j.jsg.2012.07.009>
- Kirby, E., Whipple, K. X., Tang, W. Q., & Chen, Z. L. (2003). Distribution of active rock uplift along the eastern margin of the Tibetan Plateau: Inferences from bedrock channel longitudinal profiles. *Journal of Geophysical Research*, *108*(B4), 2217. <https://doi.org/10.1029/2001JB000861>
- Li, Z., Chen, J., Han, M., Li, Y., Cao, C., Song, S., et al. (2021). Distribution and evolution of knickpoints along the Layue River, Eastern Himalayan syntaxis. *Journal of Hydrology*, *603*, 126915. <https://doi.org/10.1016/j.jhydrol.2021.126915>
- Liedel, S., Caracciolo, L., Beltrán-Triviño, A., Restrepo, J. C., Ángel, J. D. R., & Szczerba, M. (2024). A quantitative provenance analysis (QPA) approach to quantify controls on sediment generation and sediment flux in the upper reaches of the Magdalena River (Colombia): 2. Lithological control on contribution to silt- to clay-sized fractions. *Journal of Geophysical Research: Earth Surface*, *129*(5), e2023JF007369. <https://doi.org/10.1029/2023JF007379>
- Palomares, M., & Arribas, J. (1993). Modern stream sands from compound crystalline sources: Composition and sand generation index. *Processes Controlling the Composition of Clastic Sediments*, 313–322. <https://doi.org/10.1130/SPE284-p313>
- Perron, J. T., & Royden, L. (2013). An integral approach to bedrock river profile analysis. *Earth Surface Processes and Landforms*, *38*(6), 570–576. <https://doi.org/10.1002/esp.3302>
- Resentini, A., Goren, L., Castelltort, S., & Garzanti, E. (2017). Partitioning sediment flux by provenance and tracing erosion patterns in Taiwan. *Journal of Geophysical Research: Earth Surface*, *122*(7), 1430–1454. <https://doi.org/10.1002/2016JF004026>
- Schwanghart, W., & Scherler, D. (2014). Short communication: TopoToolbox 2 – MATLAB-based software for topographic analysis and modeling in Earth surface sciences. *Earth Surface Dynamics*, *2*, 1–7. <https://doi.org/10.5194/esurf-2-1-2014>
- Vezzoli, G., Garzanti, E., Limonta, M., & Radeff, G. (2020). Focused erosion at the core of the Greater Caucasus: Sediment generation and dispersal from Mt. Elbrus to the Caspian Sea. *Earth-Science Reviews*, *200*, 102987. <https://doi.org/10.1016/j.earscirev.2019.102987>
- Weltje, G. J. (1997). End-member modelling of compositional data: Numerical statistical algorithms for solving the explicit mixing problem. *Mathematical Geology*, *29*(4), 503–549. <https://doi.org/10.1007/BF02775085>
- Whipple, K. X., DiBiase, R. A., & Crosby, B. T. (2013). 9.28 bedrock Rivers, treatise on *Geomorphology*. *Treatise on Geomorphology*, 550–573. <https://doi.org/10.1016/B978-0-12-374739-6.00254-2>
- Willett, S. D., McCoy, S. W., Perron, J. T., Goren, L., & Chen, C. Y. (2014). Dynamic reorganization of river basins. *Science*, *343*(6175), 1248765. <https://doi.org/10.1126/science.1248765>
- Wobus, C., Whipple, K. X., Kirby, E., Snyder, N., Johnson, J., Spyropoulou, K., et al. (2006). Tectonics from topography: Procedures, promise, and pitfalls, Tectonics, Climate, and Landscape Evolution. In *Geological Society of America special paper, penrose conference series* (Vol. 398, pp. 55–74). [https://doi.org/10.1130/2006.2398\(04\)](https://doi.org/10.1130/2006.2398(04))
- Yang, R., Willett, S. D., & Goren, L. (2015). In situ low-relief landscape formation as a result of river network disruption. *Nature*, *520*(7548), 526–529. <https://doi.org/10.1038/nature14354>